Heliyon 6 (2020) e05194

Contents lists available at ScienceDirect

Heliyon

journal homepage: www.cell.com/heliyon

Research article

Differentiation of periapical granuloma from radicular cyst using cone beam computed tomography images texture analysis

Catharina Simioni De Rosa [a], Mariana Lobo Bergamini [a], Michelle Palmieri [a], Dmitry José de Santana Sarmento [a], Marcia Oliveira de Carvalho [b], Ana Lúcia Franco Ricardo [c], Bengt Hasseus [d], Peter Jonasson [e], Paulo Henrique Braz-Silva [a,f,*], Andre Luiz Ferreira Costa [c]

[a] Department of Stomatology, School of Dentistry, University of São Paulo, São Paulo, Brazil
[b] Department of Physics, Institute of Technology, Paulista University (UNIP), São Paulo, Brazil
[c] Postgraduate Program in Dentistry, Cruzeiro do Sul University (UNICSUL), São Paulo, Brazil
[d] Department of Oral Medicine and Pathology, Institute of Odontology, The Sahlgrenska Academy, University of Gothenburg, Gothenburg, Sweden
[e] Department of Endodontology, Institute of Odontology, The Sahlgrenska Academy, University of Gothenburg, Gothenburg, Sweden
[f] Laboratory of Virology, Institute of Tropical Medicine of Sao Paulo, School of Medicine, University of São Paulo, São Paulo, Brazil

ARTICLE INFO

Keywords:
Pathology
Dentistry
Oral medicine
Eye-ear-nose-throat
Radiology
Medical imaging
L cone beam computed tomography
Computer-assisted diagnosis
Image processing
Computer-assisted
Periapical diseases

ABSTRACT

Objective: This study aimed to investigate the use of texture analysis for characterization of radicular cysts and periapical granulomas and to assess its efficacy to differentiate between both lesions with histological diagnosis.
Methods: Cone beam computed tomography (CBCT) images were obtained from 19 patients with 25 periapical lesions (14 radicular cysts and 11 periapical granulomas) confirmed by biopsy. Regions of interest were created in the lesions from which 11 texture parameters were calculated. Spearman's correlation analysis was performed and adjusted with Benjamini-Hochberg false discovery rate procedure (FDR <0.005).
Results: The texture parameters used to differentiate the lesions were assessed by using a receiver operating characteristic analysis. Five texture parameters were predictive of lesion differentiation for eight positions: angular second moment; sum of squares; sum of average; contrast; correlation.
Conclusion: Texture analysis of CBCT scans distinguishes radicular cysts from periapical granulomas and can be a promising diagnostic tool for periapical lesions.
Clinical significance: Texture analysis can be used in diagnostic and treatment monitoring to provide supplementary information.

1. Introduction

Dental pulp exposure due to factors such as caries lesion or coronal fracture, which causes contact with microorganisms and/or their by-products, will induce an inflammatory response which can lead to pulp necrosis. The spread of these toxic products into the periapex will cause a periapical lesion in the site, being characterized by infiltration of inflammatory cells and production of cytokines and chemokines [1,2]. Radicular cysts and periapical granulomas account for two-thirds of these asymptomatic inflammatory lesions in the anterior region of the maxilla, where they are more frequent [3,4].

Precise evaluation of periapical lesions is essential to getting an accurate diagnosis and deciding on appropriate dental intervention [5]. An objective evaluation of the images could give dentists some significant information to facilitate clinical management, since periapical granulomas are tending to heal with non-surgical root canal treatment against the radicular cyst [6, 7, 8].

It has been proven that differentiation of radicular cysts and periapical granulomas by image is not possible in intraoral radiographs [9, 10] and cone beam computed tomography (CBCT) can have a moderately accurate diagnosis depending on the size of the lesion [11].

CBCT is capable of detecting more periapical lesions (20–39%) compared to the two-dimensional radiography (2D) [12,13], thus being a more reliable and precise method for differential diagnosis of these inflammatory lesions as their boundaries can be determined with greater accuracy [14,15].

Despite the many studies trying to determine a valid diagnostic method for differentiation of radicular cysts and periapical lesions prior

* Corresponding author.
E-mail address: pbraz@usp.br (P.H. Braz-Silva).

https://doi.org/10.1016/j.heliyon.2020.e05194
Received 7 September 2020; Received in revised form 25 September 2020; Accepted 5 October 2020

Table 1. Characteristics of the lesions included in the study.

Lesion	Patient age	Gender	Diameter (mm)	Volume (mm^3)	Tooth
Radicular Cyst	38	M	7.451	280.2	46
	33	M	7.115	572.7	26
	65	F	6.273	166	25
	65	F	8.127	916.1	27
	51	F	6.135	165.9	26
	72	M	4.732	145.5	41
	24	F	5.673	226.1	17
	47	F	3.996	170.8	36
	58	M	3.053	82.96	37
	48	M	5.38	688.4	16
	48	M	7.945	376.3	37
	30	F	6.73	405.9	15
	24	M	5.719	168	46
	54	F	6.018	315.9	47
Periapical Granuloma	33	M	7.115	170.3	37
	56	F	7.093	131.1	15
	52	F	3.553	41.47	11
	52	F	2.657	32.37	21
	52	F	2.168	12.01	22
	51	F	2.833	21.97	15
	51	F	6.228	47.06	36
	47	F	6.006	286	27
	36	M	2.856	47.21	16
	58	M	4.272	30.03	35
	35	M	5.92	163.9	36

to any surgical intervention, the histological method is still known to have the greatest sensitivity and specificity for diagnosis of these lesions [6].

Texture analysis is a mathematical technique applied to 2D and 3D images for identification of complex structures involving intensity variation of image element values (pixels) acquired under certain conditions [16,17]. Among the available approaches for extracting texture parameters from an image, the one based on the gray level co-occurrence matrix has been the most used method [18]. This approach relies on counting the order of co-occurrence of brightness values in pairs of pixels at a given distance (d) and direction (ϕ), as proposed by Haralick [16].

The image statistical parameters are generated and visualized after constructing the matrix by using texture maps. In some cases, it is possible to see differences not identified on the original image and which can serve for analysis, but which no longer represent the image of the tissue in the biological point of view [19].

To our knowledge, up to now only one study investigated the texture analysis of magnetic resonance image (MRI) of periapical lesions [8]. However, the disadvantages of MRI scan in a routine clinical setting include technical complexity and high cost.

The objective of the present study was to assess the efficacy of texture analysis with CBCT for differentiation of radicular cysts and periapical granulomas.

2. Materials and methods

2.1. Ethical aspects

This study was conducted according to ethical standards defined by institutional and/or national research committees and the Helsinki Declaration of 1964, including subsequent amendments or comparable ethical standards, and approved by the University of São Paulo School of Dentistry research ethics committee under protocol number 2.097.312.

Informed consent was obtained from all the 26 patients who attended the Oral and Maxillofacial Surgery Clinics of the Oral and Maxillofacial Surgery Clinics of the School of Dentistry Foundation, University of Sao Paulo. Patients with diagnosis of periapical lesion, confirmed by clinical (no response to thermal tests) and intraoral radiographs (radiological characteristics such as well-circumscribed radiolucency with sclerotic border and diffuse radiolucency with ill-defined border), with indication for dental extraction and with no metal associated (e.g. metallic posts and metal restorations) were included in the study.

2.2. Image acquisition

All the CBCT images were acquired by using a ProMax 3D scanner (Planmeca Oy, Helsinki, Finland) operating with the following parameters: 96 kVp, 12 mA, FOV (field of view) of 6 cm, voxel size of 200 μm and acquisition time of 12s.

2.3. Surgical pathology diagnosis

After acquisition of the images, the patients underwent the dental extraction. The lesions were removed, with or without the affected tooth, conditioned in 10% buffered formalin for histological processing and sent to the Oral and Maxillofacial Surgical Pathology Service of the Department of Stomatology, School of Dentistry, University of São Paulo. Histopathological analysis was performed by an experienced oral and maxillofacial pathologist, who used light microscopy to examine slides stained with hematoxylin and eosin. Periapical granulomas presenting epithelium were excluded in order to discard epithelized granulomas. Data on age, gender, lesion's location, lesion's time of evolution, symptoms, radiographic characteristics and patient's previous medical history were also collected from the patients' records.

2.4. Patients' characteristics

Of the original sample of 26 subjects, 19 patients with 25 periapical lesions were included in the study. Seven patients were excluded from the study, namely: two did not attend the sessions for tooth extraction,

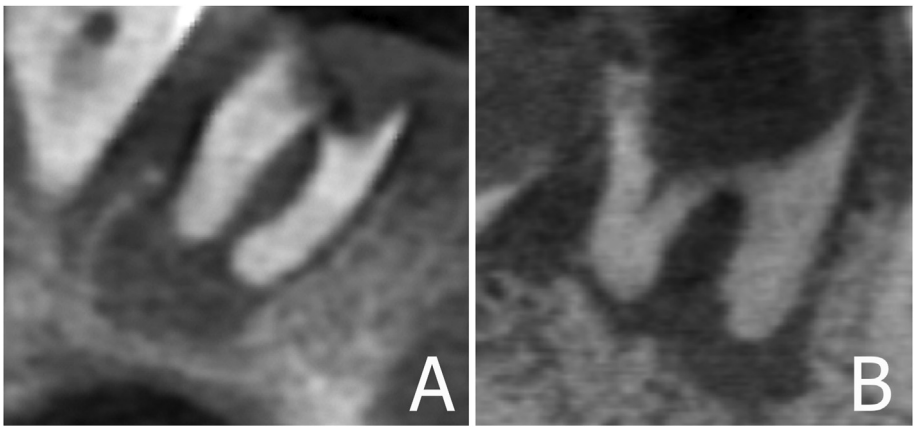

Figure 1. Example of two cases of lesions on CBCT images: A, radicular cyst; B, periapical granuloma.

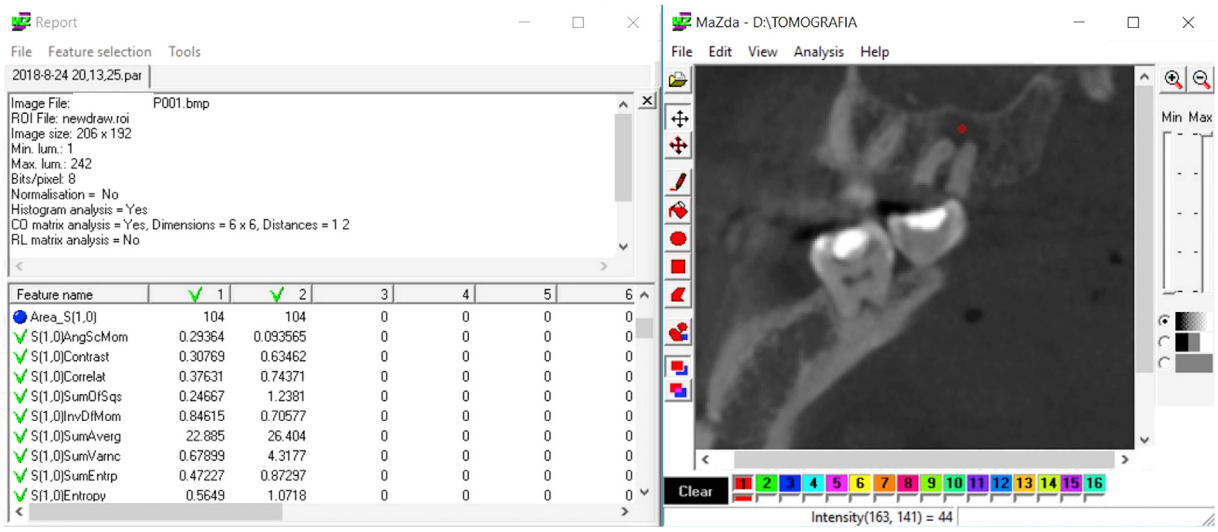

Figure 2. Sagittal CBCT image showing ROIs for analysis of the lesions by using the MaZda software. The image shows a radicular cyst.

two had no sufficient material for histopathological analysis, two had no sufficient area to delimit the region of interest (ROI) for texture analysis and one had the presence of metallic artifacts in the CBCT scan.

Of the 19 patients included, nine were female and ten were male, with age ranging from 24 to 72 years old and a mean age of 46.7 years. Four

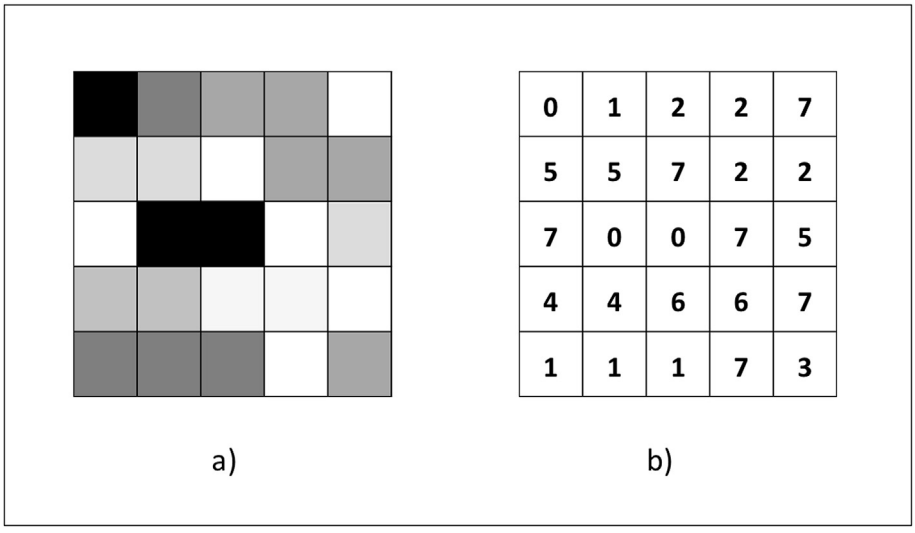

Figure 3. 5 × 5 matrix (a) with gray values corresponding numerical gray-level pixel intensities (b).

periapical lesions were found in anterior teeth and 21 in posterior teeth (Table 1).

2.5. Image analysis

The CBCT images, generated in DICOM format (Digital Imaging Communication in Medicine), were analysed by a dentomaxillofacial radiologist with 4 years' experience in CBCT imaging by using OnDemand 3D software (Cybermed Inc., Seoul, Korea). The images were evaluated on a 13.3-inch screen with 2560 × 1600 pixel resolution (Apple, Cupertino, USA) in a low-light environment. CBCT images with artifacts or any other condition affecting the image quality were excluded.

All CBCT images were displayed with WW: 1650; and WL: 875 (WW, window width; WL, window level).

Figure 1 shows CBCT images of a radicular cyst (A) and a periapical granuloma (B). The most representative sagittal views of the periapical lesions were selected (containing the largest dimension of the lesions) and then the images were converted into bitmap format (BMP).

In the process to convert from DICOM to BMP (necessary for the use of Mazda software), there is a loss of resolution. Then, the images used in the calculation of the texture parameters are two-dimensional matrices (256 × 256 pixels).

2.6. Texture analysis

An evaluator well-trained in analysing CBCT images, also blinded to clinical, histopathological and diagnostic data, performed the texture analysis. All the images were in BMP format and were exported to MaZda software [20,21] for calculating texture features.

A round-shaped ROI of 44 pixels in diameter was manually segmented and then set in the center of the lesion on the sagittal image so that only the lesion tissue was encompassed (Figure 2). The ROI definition (44 pixels) was based in the smallest lesion in our sample, ensuring enclosing area of the tissue of interest.

The gray level co-occurrence matrix is a square matrix where the number of rows and columns is equal to the number of gray levels in the image that can reveal certain properties about the spatial distribution of the gray levels in the image texture [22]. Figure 3 shows the representation of gray level co-occurrence matrix for a 5 × 5 pixel image (a), with five gray levels ranging from 0 (black) to 7 (white) (b).

The following texture parameters were analysed based on the descriptors set by Haralick [16], namely: contrast, inverse difference moment, angular second moment, correlation, sum of squares, entropy, sum of average, sum of variance, sum of entropy, difference of variance and difference of entropy (Table 2). These parameters were calculated for different positions determined by two distances between pixels ($d1 = 1$, $d2 = 2$) and four image directions (i.e. horizontal, diagonal, vertical and anti-diagonal, corresponding to $\phi = 0°$, 45°, 90°, 135°, respectively), as can be seen in Figure 4.

The two distances can be arranged with the four directions in the so-called positions: S10 (d1 = 1; $\phi = 0°$), S01 (d1 = 1; $\phi = 45°$), S11 (d1 = 1; $\phi = 90°$), S1-1 (d1 = 1; $\phi = 135°$), S20 (d2 = 2; $\phi = 0°$), S02 (d2 = 2; $\phi = 45°$), S22 (d2 = 2; $\phi = 90°$), S2-2(d2 = 2; $\phi = 135°$).

Texture parameters enable us to assess the mean gray level of ROIs and the variation of their pixel values, showing the most significant

Table 2. Texture Parameters Extracted in the Analysis of CBCT scans.

Texture parameter	Description
Contrast	Represents the amount of local variation of gray level
Inverse difference moment	Homogeneity of the distribution of gray level on the image
Angular second moment	Measurement of image uniformity
Correlation	Linear measure dependence of gray level between neighboring pixels
Sum of squares	Measurement of the dispersion (related to average) of gray level distribution
Entropy	Degree of disorder between pixels in the image
Sum of average	Mean of the distribution of the sum of gray level
Sum of variance	Dispersion around the mean of the sum distribution of gray level
Sum of entropy	Disorganization of the sum distribution of gray level
Difference of variance	Dispersion of the gray level difference
Difference of entropy	Disorganization of the gray level difference

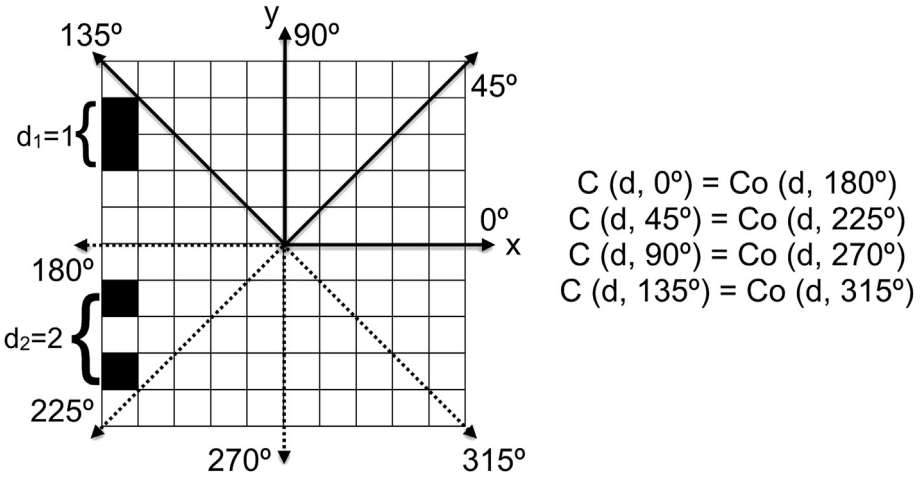

Figure 4. Representation of the acquisition of co-occurrence (C) and opposite co-occurrence (Co) values for the directions 0°, 45°, 90° and 135° and their opposites in relation to the distances d1 = 1 pixel and d2 = 2 pixels.

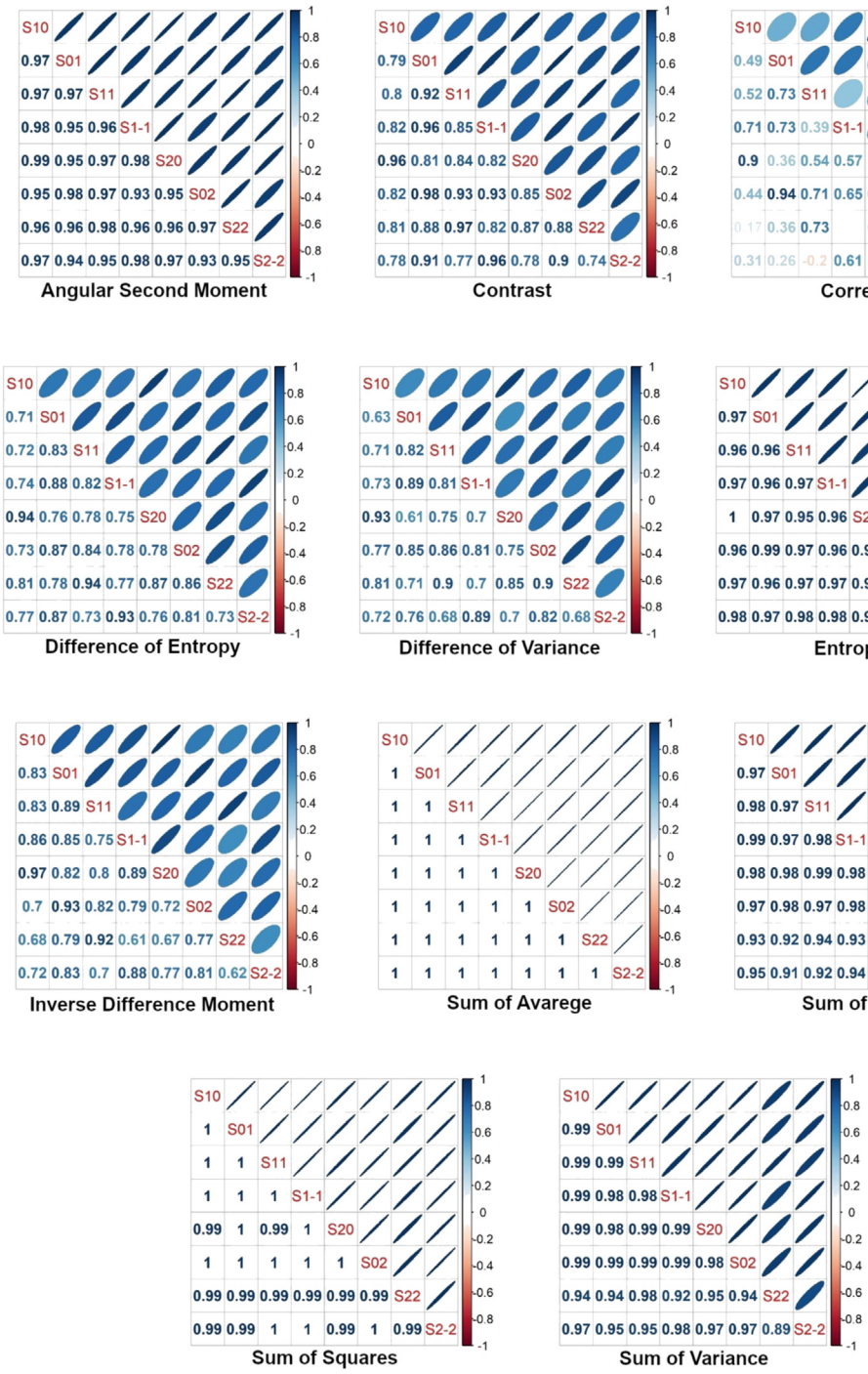

Figure 5. Correlation plots provide visual representation for the correlation between every texture parameter and the eight positions. The strength and direction of correlation are dually represented. The increasing strength is represented by the density of the colour as well as by narrowing radius of the ellipse. As such the longer diameter of the ellipses specifies a weak correlation; whereas the smaller diameter describes a strong correlation. Red and blue colors indicate positive and negative correlations, respectively. The two distances were organized with the four directions in the following positions: S10 (d1 = 1; ϕ = 0°), S01 (d1 = 1; ϕ = 45°), S11 (d1 = 1; ϕ = 90°), S1-1 (d1 = 1; ϕ = 135°), S20 (d2 = 2; ϕ = 0°), S02 (d2 = 2; ϕ = 45°), S22 (d2 = 2; ϕ = 90°), S2-2(d2 = 2; ϕ = 135°).

parameters in the comparison between the two different lesions and the histopathological diagnosis.

2.7. Statistical analysis

Statistical analysis was performed by using the R software, version 3.6.0. (The R Foundation for Statistical Computing). Spearman's correlation coefficient was used to analyse associations between the investigated parameters. Mann-Whitney's test was used to test between-groups and *P*-values were adjusted by using the Benjamini-Hochberg false discovery rate (FDR) method [23,24]. The significance level adopted was 5%.

The method to investigate the texture parameters and positions is described in the following steps:

- Eleven texture parameters were evaluated in eight different positions (88 variables). We assessed correlations between the different positions of each texture parameter and the values of correlation

coefficients that were interpreted as follows: 0.00 to 0.30 (- 0.0 to - 0.30) very weak; 0.30 to 0.50 (- 0.3 to - 0.50) weak; 0.50 to 0.70 (0.5 to - 0.70) moderate; 0.70 to 0.90 (- 0.7 to - 0.90) strong; and 0.90 to 1.00 (- 0.9 to - 1.00) very strong.

- Diagnostic performance of texture parameters significant in the differentiation of the above pathological characteristics was used in the receiver operating characteristic (ROC) curve analysis.
- Hierarchical cluster algorithm was performed by using the Euclidean distance and Ward's method. We explored which texture parameters significantly differed between radicular cysts and periapical granulomas.

3. Results

Our sample was composed of 19 patients, totalizing 25 periapical lesions, in which 14 were radicular cysts (56%) and 11 were periapical granulomas (44%).

Eleven texture parameters were evaluated in eight different positions, totalizing 88 variables. Figure 5 shows correlation plots (using the non-parametric Spearman's rank correlation coefficient) and the variance of the parameters across the eight positions. There were significant differences between the strengths of the correlations and the parameters in all positions, as follows: angular second moment, sum of squares, entropy, sum of average and sum of variance.

Each parameter was analyzed in all positions and their behaviors in any position were the same. Thus, we chose position S10 at random, since any position would present the same result (Figure 6). Statistical analysis identified, in Figure 6, pairs of parameters with similar behaviour and strong correlation: angular second moment x inverse difference moment, sum of variance x sum of squares; sum of entropy x sum of variance, sum of entropy x entropy, sum of squares x entropy, and contrast x difference of entropy.

To continue the analysis, we selected from the 11 parameters those with potential predictive ability based on statistical significance in Figures 5 and 6.

In Figure 6, with various pairwise correlations are expected to involve a great degree of redundancy. It is possible to observe that there is a strong correlation between angular second moment and inverse difference moment in S10 position. Then we left only angular second moment in S10 direction. There is a strong correlation between sum of variance and sum of squares, but also between sum of entropy and sum of variance and between sum of squares and entropy, so we left with only sum of squares in S10 position.

Sum of average did not show high correlation with any other parameter in Figure 6. Therefore, it is a parameter that should be analyzed.

The correlate and contrast parameters showed a moderate correlation between positions (Figure 4) and low correlation with the other parameters, Therefor, we choose to explore them in all directions to verify their performance for the classification of the lesions.

Five parameters were selected for the last analysis: angular second moment, sum of squares, sum of average (in the S10 direction) and contrast, with correlations in all directions.

The ROC curve was constructed to assess the discriminative performance of the five parameters chosen. Table 3 shows the comparison between the groups concerning the texture parameters selected for analysis. Mann-Whitney's test was used to compare the groups. The largest areas under the ROC curves (AUC) with values greater than 50% (the optimal cutoff threshold) were selected, given their potential to differentiate the two lesions based on their sensitivity and specificity.

As an example of the interpretation of Table 3, consider the correlation between the position S (1.0) and the parameter angular second moment. One can note that the value of this correlation is greater in the group of radicular cysts than in the group of periapical granulomas, with a statistically significant difference between them (P-value = 0.009). The area under the curve is 81.2% and the cutoff point is 0.10, showing that the position S (1.0) for the angular second moment had values greater than 0.10, meaning the presence of radicular cysts with specificity (percentage of true negatives) of 54.5% and sensitivity (percentage of true positives) of 100%. The best texture parameters for diagnoses were chosen combining when AUC value was closer to 100%, indicating the best accuracy, and statistically significant P.

Five texture parameters were predictive for differentiation of lesions, namely: angular second moment (P = 0.021, position S1.0), sum of squares (P = 0.019, position S1.0), sum of average (P = 0.019, position S1.0), contrast (P = 0.019, position S0.1), contrast (P = 0.030, position S1,1), contrast (P = 0.019, position S1.-1), contrast (P = 0.019, position S0.2), contrast (P = 0.038, position S2.2), contrast (P = 0.019, position S2.-2), correlation (P = 0.019, position S1.0), correlation (P = 0.037, position S0,1), correlation (P = 0.027, position S1.-1), correlation (P = 0.025, position S2.0) and correlation (P = 0.028, position S0.2).

Dendrograms (Figure 7) for cluster analysis using textural parameters (chosen in the previous analysis) automatically classified the lesions into two groups: one with 18 lesions and another with seven, determining the first group as radicular cysts and the second as periapical granulomas. However, compared to histopathological results, five lesions were classified incorrectly in the first group and one lesion was misclassified in the second group.

4. Discussion

Texture analysis has been used to extract useful parameters from images mostly overlooked by the human eye. In this study, we assessed the capacity of parameters extracted from ROIs on CBCT images to distinguish radicular cysts from periapical granulomas. Even with a decrease in resolution when the images are converted into BMP, there is still a lot of information that is not perceptible in the visual analysis (which distinguishes approximately 64 gray levels) [25].

The reliability of computer-aided diagnosis systems has been studied recently in the diagnosis of maxillofacial radiolucent lesions and

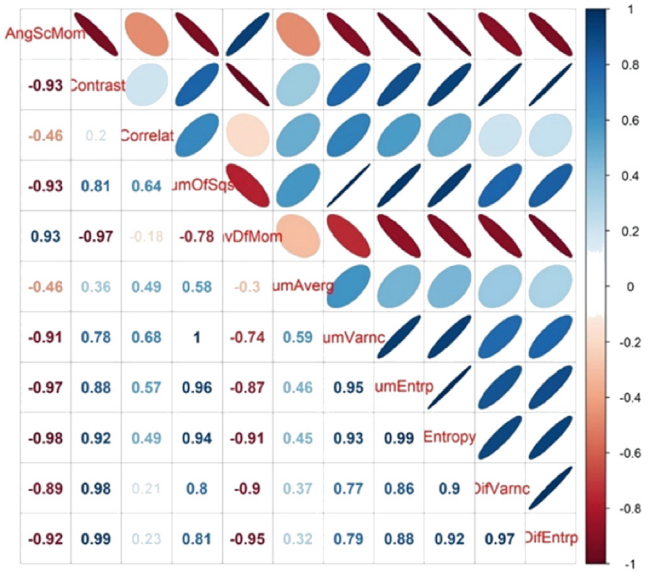

Figure 6. Correlation plot illustrates the Spearman test coefficient between the texture parameters across the position S10. The direction of the correlation (positive or negative) is represented by the colour of the ellipse (blue is positive correlation; red is negative correlation), as well as its orientation (ellipses angled up and to the right represent positive correlations). A wider ellipse indicates a weak correlation and a narrower ellipse displays a strong correlation. *AngScMom: angular second moment; Contrast: contrast; Correlat: correlation; SumOfSqs: sum of squares; InvDfMom: inverse difference moment; SumAverg: sum of average; SumVarnc: sum of variance; SumEntrp: sum of entropy; Entropy: entropy; DifVarnc: difference of variance; DifEntrp: difference of entropy.*

Table 3. Position and dispersion measures of the selected texture parameters by group. P-value of comparison between groups (p). area under the ROC curve (AUC), cutoff value and cutoff specificity and sensitivity data can be observed.

Texture Parameter	Position	Lesion	N	p	AUC	Cutoff Value	Specificity	Sensitivity
Angular Second Moment	S1.0	Cyst	14	**0.021**	81.2	0.10	54.5	100.0
		Granuloma	11					
Sum Of Squares	S1.0	Cyst	14	**0.019**	86.4	0.90	81.8	85.7
		Granuloma	11					
Sum Of Average	S1.0	Cyst	14	**0.019**	83.8	30.80	90.9	78.6
		Granuloma	11					
Contrast	S1.0	Cyst	14	0.082	71.8	-	-	-
		Granuloma	11					
	S0.1	Cyst	14	**0.019**	83.4	0.70	72.7	92.9
		Granuloma	11					
	S1.1	Cyst	14	**0.030**	77.9	0.70	81.8	85.7
		Granuloma	11					
	S1.-1	Cyst	14	**0.019**	84.4	1.10	63.6	100.0
		Granuloma	11					
	S2.0	Cyst	14	0.132	68.5	-	-	-
		Granuloma	11					
	S0.2	Cyst	14	**0.019**	82.1	1.10	81.8	85.7
		Granuloma	11					
	S2.2	Cyst	14	**0.038**	76.0	2.00	63.6	85.7
		Granuloma	11					
	S2.-2	Cyst	14	**0.019**	82.8	2.00	63.6	92.9
		Granuloma	11					
Correlation	S1.0	Cyst	14	**0.019**	83.1	0.80	72.7	100.0
		Granuloma	11					
	S0.1	Cyst	14	**0.037**	76.6	0.60	100.0	42.9
		Granuloma	11					
	S1.1	Cyst	14	0.132	68.8	-	-	-
		Granuloma	11					
	S1.-1	Cyst	14	**0.027**	79.2	0.60	81.8	78.6
		Granuloma	11					
	S2.0	Cyst	14	**0.025**	79.9	0.50	63.6	100.0
		Granuloma	11					
	S0.2	Cyst	14	**0.028**	78.6	0.30	90.9	71.4
		Granuloma	11					
	S2.2	Cyst	14	0.342	61.7	-	-	-
		Granuloma	11					
	S2.-2	Cyst	14	0.412	59.8	-	-	-
		Granuloma	11					

N: number of lesions; AUC: Area under curve; P: p value.

concluded that the current published evidence supports the accuracy of these methodologies in classifying the lesions compared to histopathological biopsy [26]. In this review, two interesting researches [14,27] discussed combined graph-based random walks segmentation with machine learning-based boosted classifiers to diagnose periapical cyst and periapical granuloma. It was measured a set of 8 features computed from the lesion's intensity distribution and fed the features to AdaBoost. However, the authors reported the complexity of the methodology for dentists and the long execution time.

Tiny changes in gray level of the images cannot be detected by eyes because they cannot recognize slight variations in the gray level, in addition to the size of the pixels [25]. We hypothesized that due to the diverse components of both lesions and their different densities, these could be reflected by their pixel intensities on CBCT images.

Previously radiometric methodology of radiograms was proposed to differentiate between periapical granulomas and cysts using digitized conventional radiographs [28]. The study had as weaknesses the use of radiograms that were not standardized and the sample size [29].

Several studies have used texture analysis for different imaging modalities with different approaches to extract texture parameters in the detection of non-visible changes in the image [8,18,19,25,30, 31, 32, 33, 34]. For example, in one study used texture analysis to identify radicular cysts and periapical granulomas on MRI scans [8]. Despite the fact that their study has some limitations, their results suggest that texture parameters quantifying tissue heterogeneity could offer some prognostic information. Compared to MRI devices, CBCT has some highly valued advantages for diagnosis of periapical lesions, such as shorter scan time, low cost and more comfort for patients during the scanning process.

In another study, computed tomography texture analysis was used as an aid in differentiating cystic and cystic-appearing odontogenic lesions of the jaw, showing that texture parameters provided additional diagnostic performance value [35].

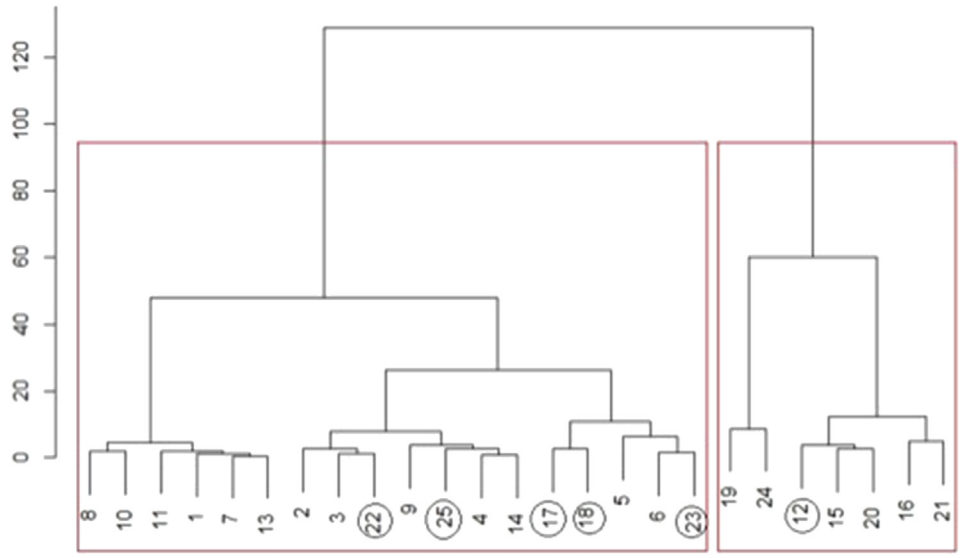

Figure 7. Dendrogram of cluster analysis of the five texture parameters, were predictive of lesion differentiation showing the separation of the lesions into two groups. Circulated lesions indicate erroneously classified.

In a recent study, the authors used gray level co-occurrence matrix-based texture analysis in CBCT images of patients with aggressive periodontitis. They concluded that there was a high diagnostic performance in the differentiation of bone tissue at the furcal lesion area and changes in regions close to it [25].

In our work, the co-occurrence matrix was set to determine changes in the gray level for two pixel distances ($d1 = 1$, $d2 = 2$) and for four angles (0^o, 45^o, 90^o, and 135^o), with eleven textural parameters to assess their ability to be a diagnostic biomarker. Thus, we generated a huge number of correlations. From that point of view, we needed to select correlations that could be linked to target lesions and decrease the number of data to be analysed, since using many parameters can lead to over-fitting as irrelevant parameters may confuse diagnostic decisions [36].

Not all positions correlated with the parameters are suitable and effective for differentiating the two kinds of lesions. By using Spearman's correlation coefficient, these parameters were reduced to the best five ones and positions to show the most reliable discrimination between radicular cysts and periapical granulomas.

Angular second moment is highly correlated with sum of squares in which the former indicates a small number of gray levels and the latter shows higher pixel weights expressing the homogeneity of the two lesions. Sum of average indicated image brightness of image, which appears to be associated with enhancement intensity and internal enhancement patterns of the lesions. Contrast indicates changes in the gray level of pixels in the comparison between both lesions. Correlation can be computed for consecutively larger window sizes. CBCT is specific for mineralized tissue and has inherently a wide window, which explains our values.

For instance, periapical granulomas have a cell content similar to the physiological one, whereas radicular cysts have their content changed by a semi-solid necrotic material resulting from liquefaction of epithelial cells [3].

The five parameters were selected for ROC curve as they achieved the area under the ROC curve of 81.2% in the other half validation set. The consistency of the selected parameters for these two models revealed the robustness of this methodology. However, because this approach was not totally perfect, the ultimate performance should be tested with a larger dataset by using cluster analysis of the selected classifiers.

Texture analysis frequently involves a complex interpretation [37]. This technique could be used by an Oral and Maxillofacial Radiologist with access to image exams at the time of the report, since these professionals have experience with image software. Once CBCT scans have been acquired, texture analysis could be recommended as an auxiliary tool in the elaboration of the report, since the subjective visual analysis is based only on the image behavior of the lesions, leaving gaps in the diagnosis.

The potential of CBCT in texture analysis still requires to be investigated especially because image quality of CBCT is commonly inferior compared to conventional computed tomography images [38,39].

For the next steps, we intend to automate the process of segmentation and statistical analysis of the images by using the five texture parameters selected (i.e. those capable of detecting tissue variations) for reduction of the execution time and by improving the quality of experimentation.

Our study has some limitations which need to be stated. Firstly, the sample was rather small and this could have hidden potential correlations. Secondly, we only performed the texture analysis on a single slice which may not take the most characteristic section of the lesion. Future studies should be focused on validating the present approach with an augmented dataset.

5. Conclusion

Our results suggest that texture analysis of CBCT images has the potential for differentiating between radicular cysts and periapical granulomas. There was an association between the five texture parameters in the characterization of the lesions. This technique can be an auxiliary tool for diagnosis and prognosis of periapical lesions.

Declarations

Author contribution statement

C. De Rosa, Mariana Lobo Bergamini, M. Palmieri, D. Sarmento, M. de Carvalho and A. Ricardo: Performed the experiments; Analyzed and interpreted the data; Wrote the paper.

B. Hasseus, P. Jonasson, P. Braz-Silva and A. Costa: Conceived and designed the experiments; Analyzed and interpreted the data; Contributed reagents, materials, analysis tools or data; Wrote the paper.

Funding statement

This work was supported by the Sao Paulo Research Foundation (FAPESP) (2009/53982-0 and 2017/09550-4).

Competing interest statement

The authors declare no conflict of interest.

Additional information

No additional information is available for this paper.

Acknowledgements

The authors would like to thank José Tadeu Sales for the language correction of the manuscript.

References

[1] T.A. Silva, G.P. Garlet, V.S. Lara, W. Martins Jr., J.S. Silva, F.Q. Cunha, Differential expression of chemokines and chemokine receptors in inflammatory periapical diseases, Oral Microbiol. Immunol. 20 (5) (2005) 310–316.
[2] P.H. Braz-Silva, M.L. Bergamini, A.P. Mardegan, C.S. De Rosa, B. Hasseus, P. Jonasson, Inflammatory profile of chronic apical periodontitis: a literature review, Acta Odontol. Scand. 77 (3) (2019) 173–180.
[3] A.L. Andrade, C.F. Nonaka, M.A. Gordon-Nunez, A. Freitas Rde, H.C. Galvao, Immunoexpression of interleukin 17, transforming growth factor beta1, and forkhead box P3 in periapical granulomas, radicular cysts, and residual radicular cysts, J. Endod. 39 (8) (2013) 990–994.
[4] I.V. Bracks, L. Armada, L.S. Goncalves, F.R. Pires, Distribution of mast cells and macrophages and expression of interleukin-6 in periapical cysts, J. Endod. 40 (1) (2014) 63–68.
[5] G. Sonmez, K. Kamburoglu, F. Yilmaz, C. Koc, E. Baris, A. Tuzuner, Versatility of high resolution ultrasonography in the assessment of granulomas and radicular cysts: a comparative in vivo study, Dentomaxillofacial Radiol. 48 (6) (2019) 20190082.
[6] P.N. Nair, New perspectives on radicular cysts: do they heal? Int. Endod. J. 31 (3) (1998) 155–160.
[7] P.N. Ramachandran Nair, G. Pajarola, H.E. Schroeder, Types and incidence of human periapical lesions obtained with extracted teeth, Oral Surg. Oral Med. Oral Pathol. Oral Radiol. Endod. 81 (1) (1996) 93–102.
[8] A. Juerchott, T. Pfefferle, C. Flechtenmacher, J. Mente, M. Bendszus, S. Heiland, T. Hilgenfeld, Differentiation of periapical granulomas and cysts by using dental MRI: a pilot study, Int. J. Oral Sci. 10 (2) (2018) 17.
[9] S.C. White, J.P. Sapp, B.G. Seto, N.J. Mankovich, Absence of radiometric differentiation between periapical cysts and granulomas, Oral Surg. Oral Med. Oral Pathol. 78 (5) (1994) 650–654.
[10] D. Ricucci, F. Mannocci, T.R. Ford, A study of periapical lesions correlating the presence of a radiopaque lamina with histological findings, Oral Surg. Oral Med. Oral Pathol. Oral Radiol. Endod. 101 (3) (2006) 389–394.
[11] J. Guo, J.H. Simon, P. Sedghizadeh, O.N. Soliman, T. Chapman, R. Enciso, Evaluation of the reliability and accuracy of using cone-beam computed tomography for diagnosing periapical cysts from granulomas, J. Endod. 39 (12) (2013) 1485–1490.
[12] F.W. de Paula-Silva, M.K. Wu, M.R. Leonardo, L.A. da Silva, P.R. Wesselink, Accuracy of periapical radiography and cone-beam computed tomography scans in diagnosing apical periodontitis using histopathological findings as a gold standard, J. Endod. 35 (7) (2009) 1009–1012.
[13] W.G. van der Borden, X. Wang, M.K. Wu, H. Shemesh, Area and 3-dimensional volumetric changes of periapical lesions after root canal treatments, J. Endod. 39 (10) (2013) 1245–1249.
[14] K. Okada, S. Rysavy, A. Flores, M.G. Linguraru, Noninvasive differential diagnosis of dental periapical lesions in cone-beam CT scans, Med. Phys. 42 (4) (2015) 1653–1665.
[15] E. Yilmaz, T. Kayikcioglu, S. Kayipmaz, Computer-aided diagnosis of periapical cyst and keratocystic odontogenic tumor on cone beam computed tomography, Comput. Methods Progr. Biomed. 146 (2017) 91–100.
[16] R.S. Haralick, K. Dinstein, I textural features for image classification, IEEE Transact. Sys. Man Cybernetics 3 (1973) 610–621.
[17] H. R, statistical and structural approaches to texture, Proc. IEEE 67 (1979) 786–804.
[18] M. de Albuquerque, L.G. Anjos, H. Maia Tavares de Andrade, M.S. de Oliveira, G. Castellano, T. Junqueira Ribeiro de Rezende, A. Nucci, M.C. Franca Junior, MRI texture analysis reveals deep gray nuclei damage in amyotrophic lateral sclerosis, J. Neuroimaging 26 (2) (2016) 201–206.
[19] M.S. Oliveira, P.T. Fernandes, W.M. Avelar, S.L. Santos, G. Castellano, L.M. Li, Texture analysis of computed tomography images of acute ischemic stroke patients, Braz. J. Med. Biol. Res. 42 (11) (2009) 1076–1079.
[20] P.M. Szczypinski, M. Strzelecki, A. Materka, A. Klepaczko, MaZda–a software package for image texture analysis, Comput. Methods Progr. Biomed. 94 (1) (2009) 66–76.
[21] M.S. Strzelecki, P. Materka, A. Klepaczko, A MaZda - a software tool for automatic classification and segmentation of 2D/3D medical images, Nucl. Instrum. Methods Phys. Res. Sect. A Accel. Spectrom. Detect. Assoc. Equip. 702 (2013) 137–140.
[22] B. B.A.B, A. Pathak, D. Barooah, Gray-level Co-occurrence matrix implementation based on edge detection information for surface texture analysis, ACEEE (2014) 348–352.
[23] F. Mungai, G.B. Verrone, M. Pietragalla, V. Berti, G. Addeo, I. Desideri, L. Bonasera, V. Miele, CT assessment of tumor heterogeneity and the potential for the prediction of human papillomavirus status in oropharyngeal squamous cell carcinoma, Radiol. Med. (2019).
[24] H.Y. Benjamini Y, Controlling the false discovery rate: a practical and powerful approach to multiple testing, J. Roy. Stat. Soc. 57 (1995) 289–300.
[25] B.C. Goncalves, E.C. de Araujo, A.D. Nussi, N. Bechara, D. Sarmento, M.S. Oliveira, M.P. Santamaria, A.L.F. Costa, S. Lopes, Texture analysis of cone-beam computed tomography images assists the detection of furcal lesion, J. Periodontol. 91 (2020) 159–1166.
[26] V.K.S. Silva, W.A. Vieira, I.M. Bernardino, B.A.N. Travencolo, M.A.V. Bittencourt, C. Blumenberg, L.R. Paranhos, H.C. Galvao, Accuracy of computer-assisted image analysis in the diagnosis of maxillofacial radiolucent lesions: a systematic review and meta-analysis, Dentomaxillofacial Radiol. 49 (3) (2020) 20190204.
[27] R.S. Flores A, R. Enciso, K. Okada, NON-INVASIVE differential diagnosis OF dental periapical lesions IN cone-beam CT, Med. Phys. 42 (2009).
[28] M.K. Shrout, J.M. Hall, C.E. Hildebolt, Differentiation of periapical granulomas and radicular cysts by digital radiometric analysis, Oral Surg. Oral Med. Oral Pathol. 76 (3) (1993) 356–361.
[29] I. Rozylo-Kalinowska, Digital radiography density measurements in differentiation between periapical granulomas and radicular cysts, Med. Sci. Mon. Int. Med. J. Exp. Clin. Res. 13 (Suppl 1) (2007) 129–136.
[30] J.V. Raja, M. Khan, V.K. Ramachandra, O. Al-Kadi, Texture analysis of CT images in the characterization of oral cancers involving buccal mucosa, Dentomaxillofacial Radiol. 41 (6) (2012) 475–480.
[31] C.Y. Huang Yh, C.S. Huang, T.J. Wu, J.H. Chen, R.F. Chang, Computer-aided diagnosis of mass-like lesion in breast MRI: differential analysis of the 3-D morphology between benign and malignant tumors, Comput. Methods Progr. Biomed. 112 (2013) 508–517.
[32] R. Peyret, A. Bouridane, S.A. Al-Maadeed, S. Kunhoth, F. Khelifi, Texture analysis for colorectal tumour biopsies using multispectral imagery, Conf Proc IEEE Eng Med Biol Soc (2015) 7218–7221, 2015.
[33] M.S. de Oliveira, A. D'Abreu, M.C. Franca Jr., I. Lopes-Cendes, F. Cendes, G. Castellano, MRI-texture analysis of corpus callosum, thalamus, putamen, and caudate in Machado-Joseph disease, J. Neuroimaging 22 (1) (2012) 46–52.
[34] M.S. de Oliveira, L.E. Betting, S.B. Mory, F. Cendes, G. Castellano, Texture analysis of magnetic resonance images of patients with juvenile myoclonic epilepsy, Epilepsy Behav. 27 (1) (2013) 22–28.
[35] M. Oda, P.V. Staziaki, M.M. Qureshi, V.C. Andreu-Arasa, B. Li, K. Takumi, M.N. Chapman, A. Wang, A.R. Salama, O. Sakai, Using CT texture analysis to differentiate cystic and cystic-appearing odontogenic lesions, Eur. J. Radiol. 120 (2019) 108654.
[36] H. Wu, T. Sun, J. Wang, X. Li, W. Wang, D. Huo, P. Lv, W. He, K. Wang, X. Guo, Combination of radiological and gray level co-occurrence matrix textural features used to distinguish solitary pulmonary nodules by computed tomography, J. Digit. Imag. 26 (4) (2013) 797–802.
[37] I. Phillips, M. Ajaz, V. Ezhil, V. Prakash, S. Alobaidli, S.J. McQuaid, C. South, J. Scuffham, A. Nisbet, P. Evans, Clinical applications of textural analysis in non-small cell lung cancer, Br. J. Radiol. 91 (1081) (2018) 20170267.
[38] S. Mazziotti, A. Blandino, M. Gaeta, A. Bottari, C. Sofia, T. D'Angelo, G. Ascenti, Postprocessing in maxillofacial multidetector computed tomography, Can. Assoc. Radiol. J. 66 (3) (2015) 212–222.
[39] J.E. van Timmeren, R.T.H. Leijenaar, W. van Elmpt, B. Reymen, C. Oberije, R. Monshouwer, J. Bussink, C. Brink, O. Hansen, P. Lambin, Survival prediction of non-small cell lung cancer patients using radiomics analyses of cone-beam CT images, Radiother. Oncol. 123 (3) (2017) 363–369.